Ligand binding by butadiyne-linked porphyrin dimers, trimers and tetramers

Harry L. Anderson, Sally Anderson and Jeremy K. M. Sanders*
Cambridge Centre for Molecular Recognition, University Chemical Laboratory, Lensfield Road, Cambridge CB2 1EW, UK

The binding of oligopyridyl ligands to butadiyne-linked zinc porphyrin dimers, trimers and tetramers has been investigated in detail using NMR and electronic spectroscopy. Pyridine binds to zinc porphyrin monomers in CH_2Cl_2 solution at 300 K with binding constants of *ca.* 10^3 mol^{-1} dm^3, while 4,4′-bipyridyl binds to the cyclic zinc porphyrin dimer with a binding constant of 1×10^9 mol^{-1} dm^3, giving an effective molarity, or chelation factor, of 76 mol dm^{-3}. The analogous linear dimer binds to this ligand 100 times less strongly, but adopts a similar conformation when bound. *s*-Tri(4-pyridyl)triazine has an affinity of *ca.* 10^{10} mol^{-1} dm^3 for the cyclic zinc trimer, reflecting reasonably good host–guest complementarity. The affinity of 4,4′-bipyridyl for the trimer is *ca.* 10^5 mol^{-1} dm^3, implying two-point binding accompanied by host distortion and strain which reduce the binding constant; the trimer is therefore an elastic host, able to respond to the geometrical demands of rigid guests. The cyclic tetramer is a relatively flexible molecule, but its complexes with both bidentate and tetradentate ligands have more highly defined geometries. The cyclic dimer and trimer have open pre-organised cavities, with no conformational barrier to ligand binding inside the cavity, whereas the cyclic tetramer can adopt many conformations in free solution.

Introduction

We present here details of the ligand-binding properties of the porphyrin dimers, trimers and tetramers described in the preceding [1] and following [2] papers. An understanding of these properties laid the groundwork for the catalytic work which is our goal.[3–5] Some of these results have been reported previously in preliminary form.[6–8]

Our intention was to probe the shape and flexibility of the porphyrin oligomers by testing their ability to bind a range of monodentate and multidentate ligands. We have previously used a similar approach to study other porphyrin dimers.[9,10]

Fig. 1 shows a schematic view of the binding of a bidentate ligand, L–L, to a metalloporphyrin dimer, M–M. The measured binding constant for the symmetrical bifunctional ligand L–L to the dimer is $K_{LL\cdot MM}$, while the microscopic binding constant for each M–L interaction is K_1. The equilibrium constants for the two processes are $2K_1$ and $EMK_1/2$. The numerical factors arise from the fact that the ligand has two equivalent sites for binding. EM is the effective molarity or chelation factor for the second binding, which can be defined as

$$EM = K_{LL\cdot MM}/K_1^2$$

Effective molarities are a useful way of quantifying host-guest complementarity.[11] They also give an indication of the degree of rate acceleration that might be achieved if this binding energy could be directed into transition state stabilisation for a bimolecular reaction.

When considering binding of a tridentate ligand to a tritopic host we use the definition:

$$EM = \sqrt{\frac{K_{LLL\cdot MMM}}{K_1^3}}$$

Here EM is actually the square root of the product of two chelation factors. When trying to calculate an effective molarity one encounters the problem that K_1 cannot be measured directly; it is not possible to measure the affinity of just one end of L–L for M–M without doing something to prevent chelation, and any tampering with the structure is likely to affect the microscopic binding properties. It is rarely true that the

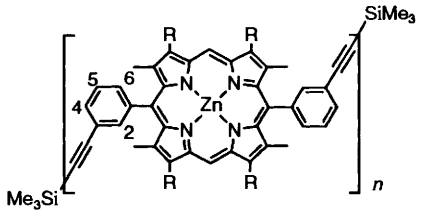

Zn-Mon1b(SiMe$_3$)$_2$ $n = 1$

Zn$_2$-l-Dim1b,c(SiMe$_3$)$_2$ $n = 2$

Zn$_4$-l-Tet1b,c(SiMe$_3$)$_2$ $n = 4$

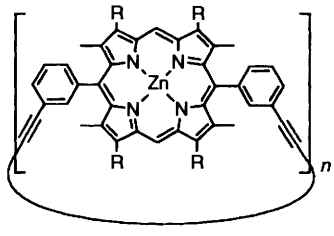

Zn$_2$-c-Dim1b,c $n = 2$

Zn$_3$-c-Tri1a,b $n = 3$

Zn$_4$-c-Tet1b,c $n = 4$

a R = CH_2CH_3

b R = $CH_2CH_2CO_2Me$

c R = 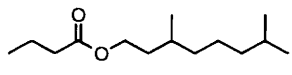

* E-mail: jkms@cus.cam.ac.uk.

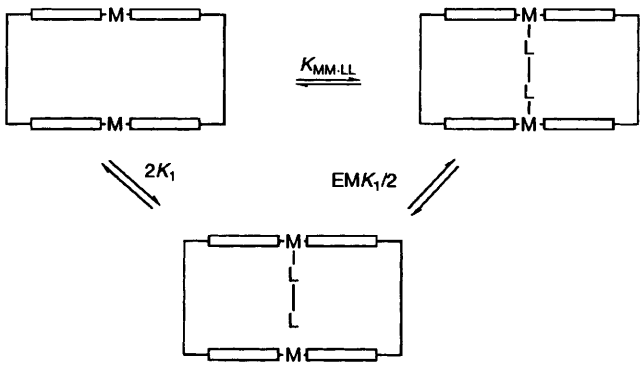

Fig. 1 Thermodynamic cycle for binding a porphyrin dimer, M–M, to a bidentate ligand, L–L

microscopic binding constant of one end of a dipyridyl ligand is the same as that of pyridine, because the basicity of pyridine is affected by substituents. It is better to approximate the microscopic binding constant of one end of a zinc–porphyrin dimer to that of the analogous monomer, because the zinc sites are further apart and so likely to behave more independently, provided that the cavity is sufficiently large. The best approach is to assume that one end of a zinc–porphyrin dimer binds any pyridine ligand more, or less, strongly than the corresponding monomer by some constant factor, so the following equation can be used to estimate the affinity of one end of the bidentate ligand, L–L, for one end of the dimer, M–M:

$$K_1 = \frac{K_{LL\cdot MM}}{2} \cdot \frac{K_{L\cdot MM}}{K_{L\cdot M}}$$

It is possible to estimate how large effective molarities might be if host–guest complementarity were perfect. In the absence of entropic solvent effects the effective molarity for the formation of a strain-free chelate L–L·M–M is

$$EM_{max} = \exp\left(\frac{\Delta S^{Trans} + \Delta S^{Vib}_{LL} - 2\Delta S^{Vib}_{L}}{R}\right)$$

where ΔS^{Trans} is the rotational and translational entropy of a ligand molecule in free solution (190 ± 20 J mol^{-1} K^{-1}). ΔS^{Vib}_{LL} and ΔS^{Vib}_{L} are the vibrational entropies gained on formation of the LL·MM and L·M complexes, respectively. The entropy of formation of the L·M complex, ΔS_{ML}, is the difference between the vibrational entropy gained, ΔS^{Vib}_{L}, and the translational energy lost, ΔS^{Trans}, thus

$$\Delta S_{ML} = \Delta S^{Vib}_{L} - \Delta S^{Trans}$$

Entropies for forming zinc porphyrin–pyridine complexes in dichloromethane are around 40–50 J mol^{-1} K^{-1};[12,13] most of the translational entropy of the pyridine is not lost when it binds, but just transformed into vibrational entropy in the new Zn–N bond. The vibrational and rotational entropy of the monodentate ligand L in L·M is likely to be similar to that of the bidentate ligand LL in LL·MM, so $\Delta S^{Vib}_{L} \approx \Delta S^{Vib}_{LL}$. So the effective molarity can be expressed as

$$EM_{max} = \exp\left(\frac{\Delta S_{ML}}{R}\right)$$

This implies that a strain-free chelate between a porphyrin dimer host and a perfectly complementary dipyridine should exhibit a maximum effective molarity in the region of 100–400 mol dm^{-3}. The measured effective molarities for complexes such as **BiPy·Zn$_2$-c-Dim1b** reported in this paper are within an order of magnitude of this, implying that the stabilities of these complexes are limited more by the looseness of the zinc porphyrin–pyridine interaction than by the imperfection of the shape complementarity between host and guest. Higher chelation factors could probably be obtained by using more basic amine ligands, by using electron-withdrawing substituents to make the zinc porphyrin more electrophilic, by using more strongly coordinating metals (such as ruthenium) or by working in less polar solvents, such as cyclohexane.

Binding processes were followed by ^{1}H NMR and electronic spectroscopies. NMR was used to study the structure of the ligand–porphyrin complexes, mainly by interpretation of the porphyrin-induced ring-current shifts experienced by bound ligands. NMR also provided qualitative thermodynamic information through observation of exchange rates for the equilibrium:

$$\text{Porphyrin} + \text{Ligand} \rightleftharpoons \text{Complex}$$

As a rough guide for our systems, where complexation shifts are often several ppm, slow exchange is observed when the binding constant exceeds around 10^7 mol^{-1} dm^3, and fast exchange when the binding constant is less than 10^5 mol^{-1} dm^3; intermediate binding constants give highly exchange-broadened signals.[14] In the case of slow exchange complexes, ^{1}H NMR was used to analyse quantitatively mixtures of cyclic porphyrin hosts competing for a given amine ligand.

Accurate binding constants can be measured by NMR titration in weakly binding cases in the fast exchange regime but following titrations by electronic spectroscopy is quicker and can be applied to a wider range of binding constants. The thermodynamic data from such titrations allow structural deductions which complement the chemical shift information from NMR. UV–VIS spectra of systems in dynamic equilibrium are 'in slow exchange', so the observed spectrum is the sum of the spectra for free and bound species. In our zinc porphyrin system the Soret band is red shifted by *ca.* 14 nm on binding a pyridine ligand, which is comparable to the peak width. Binding constants were extracted from changes in absorption at particular wavelengths by computer simulation of binding curves.

Results and discussion

Synthesis

The structures of the porphyrin hosts are illustrated above. The best syntheses of these hosts rely on a templated approach that uses the binding properties presented in this paper.[2]

All the ligands are commercially available except *s*-tri(4-pyridyl)triazine, **Py$_3$T**, and 4′-phenyl-4,2′:6′,4″-terpyridyl, **Py$_2$Py**. The published synthesis of **Py$_3$T** by action of strong base on 4-cyanopyridine requires inconveniently high pressures,[15] but we found that the reaction can be carried out in 71% yield by using 18-crown-6 and potassium hydroxide in refluxing decalin. The previously unknown phenylterpyridyl ligand **Py$_2$Py** was synthesised in 6% yield by BF_3-catalysed condensation of 4-acetylpyridine with benzaldehyde, followed by treatment with ammonium acetate, as shown in Scheme 1.[16,17] This reaction also produces the isomeric compound 2′-phenyl-4,4′:6′,4″-terpyridyl in 5% yield; the two terpyridines were separated by flash chromatography.

UV–VIS spectroscopic methods for measuring binding constants

Binding constants in dichloromethane at 27–30 °C were determined using the procedures detailed in the Experimental section. Titrations were carried out at constant porphyrin concentration, making it easy to inspect the the spectra for isosbesticity and simplifying analysis of the data. Binding constants were determined from the titration curves using a simplex least-squares curve-fitting program.[18]

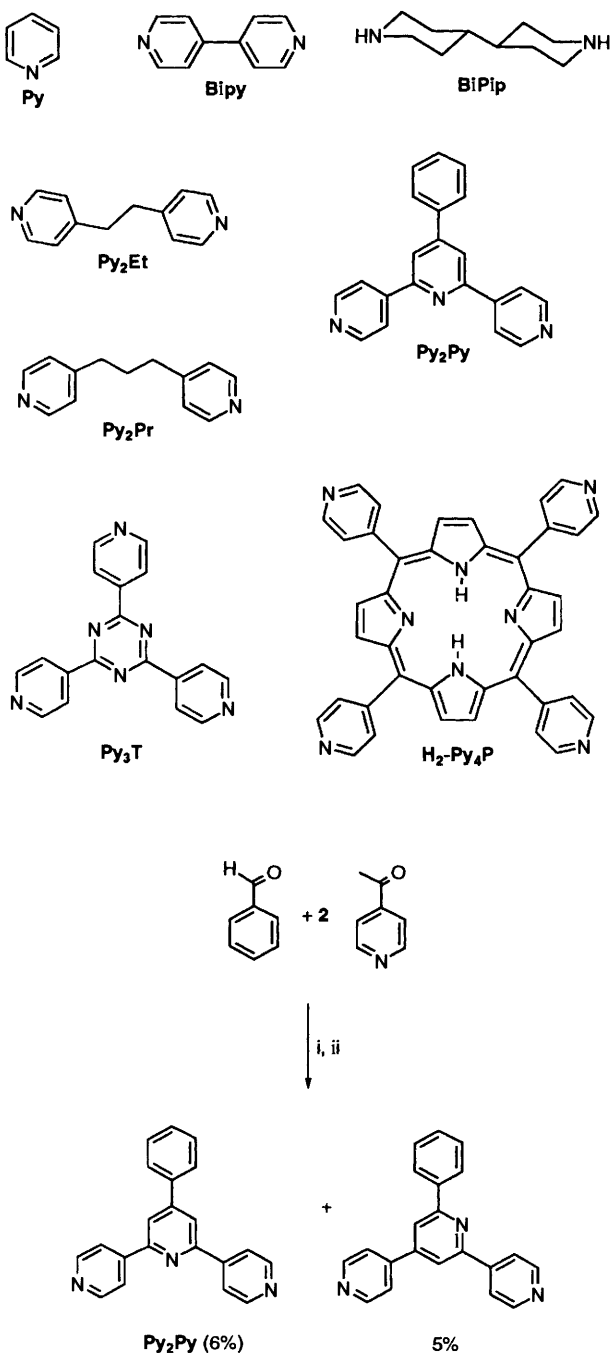

Scheme 1 (i) BF_3·Et_2O (ii) NH_4OAc, AcOH

In the some cases binding curves are biphasic, but most of these have one binding constant, K_1, which is several orders of magnitude stronger than the other, K_2, so each binding constant is manifested over a different concentration range. Such situations are best treated by carrying out two separate titrations since the optimum concentration for measuring K_1 is different from that for measuring K_2, so each data set was analysed for a single binding constant.

Care was taken to develop titration methods which minimised both random and systematic errors. This was particularly important for cases where strong binding ($> 10^7$ mol^{-1} dm^3) necessitated the use of extremely dilute solutions. The changes in absorption were monitored as a function of concentration at the two wavelengths at which maximum change in absorption occurred during the titration. Each UV titration produces two data sets; one for the declining absorption near λ_{max} of the free host and one for the rising absorption near λ_{max} of the complex. The data sets can be analysed separately to give two estimates of the binding constant, which can be averaged. However it is both more accurate and more convenient to subtract one data set from the other, and then carry out the simulation analysis on the combined data set. This subtraction eliminates errors due to slow random drift in the base-line since such effects cause a simultaneous rise and fall in the absorption at both wavelengths. Errors of this type have a negligible effect on the accuracy when one is using strong solutions, but they can become substantial when carrying out titrations at extremely low concentration, when measuring very strong binding constants, as illustrated by Fig. 2.

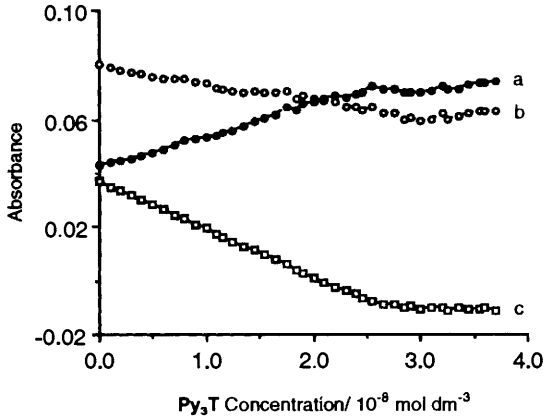

Fig. 2 UV binding curves for titration of **Zn_3-c-Tri1a** with **Py_3T**. (*a*) absorbance at 423 nm (*b*) absorbance at 410 nm (*c*) the difference b − a.

The binding constants in Table 1 are empirical values. These can be converted into microscopic binding constants by dividing by the appropriate statistical factors.[19] For example, the microscopic binding constants of **Bipy** and **Py_3T** for **Zn-Mon1a** are calculated by dividing the empirical values by 2 and 3, respectively. However, when calculating the microscopic binding constant of **Zn_3-c-Tri1a** for pyridine it is *not* correct to divide the empirical value by 3. This difference arises because weak binding constants are measured under conditions of an excess of ligand. The binding constant between **Zn-Mon1a** and **Py_3T** was measured in the presence of an excess of ligand and it reflects predominantly formation of the 1 : 1 complex, which is nine times as stable as **Py_3T·[Zn-Mon1a]$_3$** whereas the binding constant for **Py** and **Zn_3-c-Tri1a** is a weighted average of the stability constants of **Zn_3-c-Tri1a·Py**, **Zn_3-c-Tri1a·[Py]$_2$** and **Zn_3-c-Tri1a·[Py]$_3$**; it is already the same as the microscopic binding constant. The binding curves for cyclic tetramer **Zn_4-c-Tet1b** and bidentate ligands (**BiPy** and **BiPip**) were analysed to yield empirical binding constants; to do this the cyclic tetramer was treated as two dimer units which behave independently (or with complete cooperativity when binding). The ester functionalised porphyrins (series **b**) generally gave complexes with slightly (but genuinely) higher binding constants than the ethyl substituted porphyrins (series **a**), presumably as a result of the electron-withdrawing carbonyl groups.† With monomeric porphyrins **Zn-Mon1a** and **Zn-Mon1b**, binding constants differ by a factor of 0.7–0.5.[20]

Table 2 summarises the binding properties of the linear and cyclic porphyrin oligomers in effective molarity terms. Effective molarities are the product of several experimental binding constants, so the values are only approximate (± ~ 50%).

† Nitration of the *meso*-positions, or *meso*-oxidation to the dioxoporphyrin, gives 10–100 fold increases in binding affinity.[21]

Table 1 Empirical ligand affinities (in mol^{-1} dm^3) of porphyrins in CH_2Cl_2 at 30 °C

	Py	BiPy	Py_2Et	Py_2Pr	Py_2Py	Py_3T	H_2-Py_4P
Zn-Mon1a	2.8×10^3	4.7×10^3	8.5×10^3	1.1×10^4	6.2×10^3	3.9×10^3	—
Zn-Mon1b	5.2×10^3	8.4×10^3	1.2×10^4	1.7×10^4	1.2×10^4	7.6×10^3	—
Zn_2-c-Dim1b	4.5×10^3	1×10^9	1.4×10^6	1.2×10^5	5.7×10^3	6.8×10^3	—
Zn_2-l-Dim1b($SiMe_3$)$_2$	—	6×10^6	—	—	—	—	3×10^6
Zn_3-c-Tri1a	2.7×10^3	6.0×10^4	1.3×10^7	1.5×10^8	1.1×10^8	9×10^9	—
		4.5×10^3	3.4×10^3	6.2×10^4	1.6×10^4		
Zn_3-c-Tri1b	4.4×10^3	8.3×10^4	3.1×10^7	6.1×10^8	5.4×10^8	4×10^{10}	—
		9×10^3	1.0×10^4	1.2×10^4	3.6×10^4		
Zn_2H_2-c-Tri1a	2×10^3	1.6×10^4	4.5×10^6	—	—	4.4×10^7	—
Zn_4-c-Tet1b	—	2.0×10^8	—	—	—	—	2×10^{10}
Zn_4-l-Tet1b($SiMe_3$)$_2$	—	7.0×10^6	—	—	—	—	7×10^9

Table 2 Chelation factors (EM/mol dm^{-3}) of zinc porphyrin oligomers

Ligand	BiPy	Py_2Et	Py_2Pr	Py_2Py	Py_3T	H_2Py_4P
Zn_2-c-Dim1b	76	0.052	0.0022			
Zn_2-l-Dim1b($SiMe_3$)$_2$	0.5					
Zn_3-c-Tri1a	0.012	0.77	5.4	11	2.1	—
Zn_3-c-Tri1b	0.0063	1.2	12	21	2.8	—
Zn_2H_2-c-Tri1a	0.0034	0.29	—	—	30	—
Zn_4-c-Tet1b	16	—	—	—	—	0.003
Zn_4-l-Tet1b($SiMe_3$)$_2$	0.5	—	—	—	—	0.0008

Binding properties of the cyclic dimer

Although the cyclic dimer has more than one binding site, the binding curve with pyridine can be analysed accurately in terms of just three parameters: a single binding constant and two absorption coefficients (for fully bound and fully unbound host). This shows that each binding site is behaving independently; if binding at one site were to affect the ligand affinities or absorption properties of other sites then the binding curve would be more complicated. Furthermore, the empirical binding constant is very similar to that of the monomer **Zn-Mon1b**, indicating that there is no hindrance to binding inside the cavities of this host; any barrier to pyridine entering the cavities would make the binding constant less than that of the monomer.

All the bidentate ligands, except **Py_2Py**, bind much more strongly to **Zn_2-c-Dim1b** than to **Zn-Mon1b**. **Py_2Py** is clearly too big to fit into the cavity, as confirmed by CPK models, but the other ligands are either flexible enough, or small enough, to bind both zinc atoms simultaneously. The chelation factor of the **Zn_2-c-Dim1b·BiPy** complex is 76 mol dm^{-3}, which is unusually high for a complex of this type, although the zinc porphyrin dimer of Sutherland and Danks[22] has a similar affinity for **BiPy**. This behaviour is quite different from that of the flexible porphyrin dimers studied previously in our laboratory;[23] these had microscopic pyridine binding constants of less than half those of their monomeric analogues, because they adopted closed conformations, so that only one face of each porphyrin was available for binding. Even the exposed face had reduced ligand affinity because interaction with the π-electrons of the other porphyrin reduced the electrophilicity of the metal. Both UV and ^1H NMR titrations show that **Zn_2-c-Dim1b** binds **BiPy** much more strongly than **Py_2Et**. **Py_3T** has a similar donor-set geometry to **Py_2Py** and is also too large to chelate; it binds similarly to both **Zn_2-c-Dim1b** and **Zn-Mon1b**.

Apart from **BiPy**, all the ligands gave broad fast-exchange ^1H NMR spectra with **Zn_2-c-Dim1b**. Titration of **Zn_2-c-Dim1b** with **BiPy** confirmed that a very stable 1 : 1 complex is formed; **BiPy·Zn_2-c-Dim1b** is in slow exchange with an excess of either component at room temperature. The chemical-shift changes accompanying complexation are shown in Fig. 3(*a*). Model building indicates that **BiPy** is *ca.* 1 Å too short to fit the relaxed cavity of the dimer. However, the small shifts at the *meso* position and ring methyls indicate that the distance between the porphyrins does not change significantly when **BiPy** binds. The large upfield shifts at the internal aromatic proton 2-H of the host (0.72 ppm) and the downfield shift of the external proton 6-H *ortho* to the porphyrin (0.22 ppm) indicate that the aryl groups are bent more-out-of-the-plane of the porphyrin in the complex, which might imply that the porphyrins move further apart on formation of the complex. The increased porphyrin deformation in the complex may reflect the increased flexibility of the five-coordinate zinc porphyrin which allows the strained butadiyne groups to relax. The upfield shifts of the α and β-protons of the guest are unusually large since they are shielded by both porphyrins.

A ROESY spectrum ‡ of a mixture of **BiPy·Zn_2-c-Dim1b** and free **BiPy** detected NOE cross-peaks between both protons of the bound ligand and the internal *ortho*-aromatic protons of the host, as well as between host resonances. Chemical exchange cross-peaks were also detected between the free and bound ligand resonances; these are distinguished from genuine NOE peaks by their sign, which is the same as that of the diagonal and opposite to that of NOE peaks. The detection of exchange cross-peaks demonstrates that although exchange is slow on the chemical shift time-scale (there is no broadening at room temperature), it is fast on the T_1 time-scale.

Binding properties of the linear dimer

The binding constants between the linear dimer **Zn_2-l-Dim1b($SiMe_3$)$_2$** and **BiPy** and **H_2-Py_4P** were measured by UV–VIS spectroscopy and found to be 6×10^6 mol $^{-1}$ dm^3, and 3×10^6 mol $^{-1}$ dm^3, respectively (see Table 1). In the latter case the binding was assumed to be statistical and the data analysed for simple 1 : 1 association. ^1H NMR spectroscopic evidence

‡ This spin-locked version of the NOESY experiment is required to detect magnetisation transfer in medium-sized molecules such as **BiPy·Zn_2-c-Dim1b** with tumbling rates near the zero NOE regime.[14]

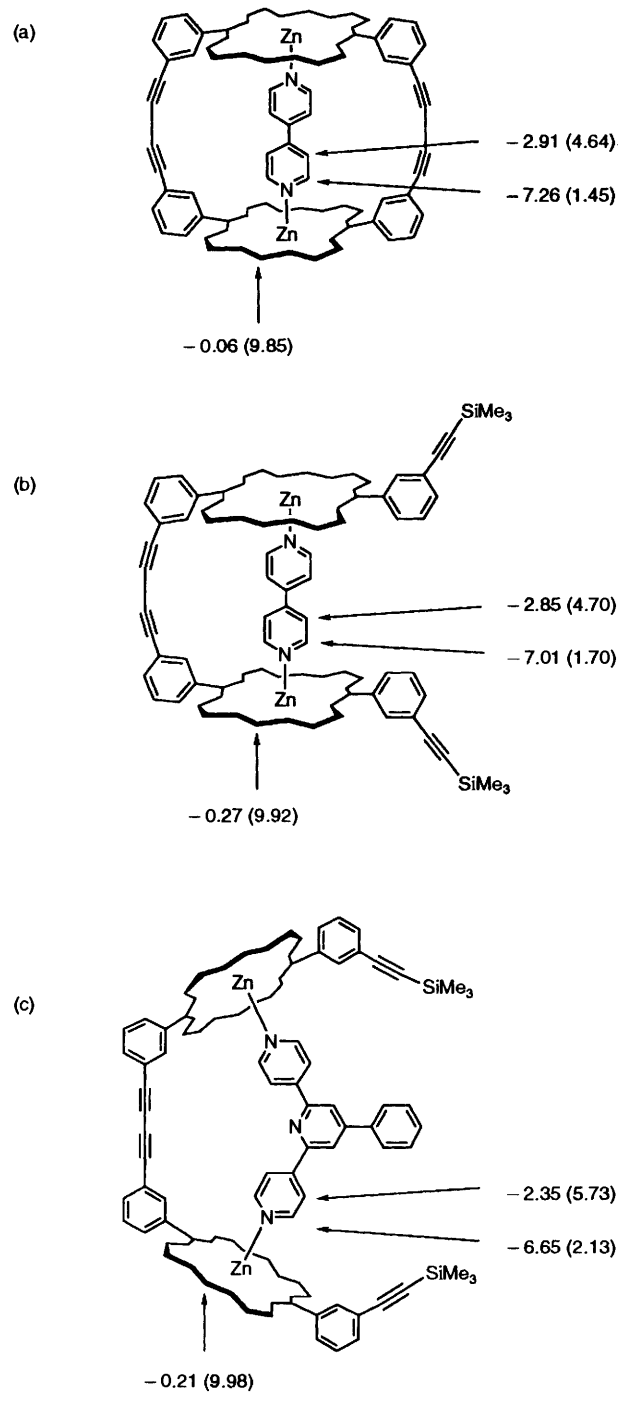

Fig. 3 Changes in ^{1}H NMR chemical shifts on formation of the complexes between: (*a*) **Zn_2-c-Dim1b** and **BiPy**; (*b*) **Zn_2-1-Dim1b-($SiMe_3$)$_2$** and **BiPy** (*c*) **Zn_2-1-Dim1b($SiMe_3$)$_2$** and **Py_2Py**. Actual chemical shifts are in parenthesis.

suggests that **BiPy** and the linear dimer **Zn_2-l-Dim1b($SiMe_3$)$_2$** form a stable 1 : 1 complex: the bound ligand signals remain sharp until an excess of the ligand had been added. Fig. 3(*b*) shows some of the changes in chemical shift when **BiPy** binds to the linear dimer in deuteriochloroform. When these chemical-shift changes are compared with those accompanying complexation of cyclic dimer by **BiPy** [Fig. 3(*a*)] some useful parallels can be drawn and information on the geometry of the complex obtained. For example, consider the *meso* region. In **Zn_2-l-Dim1b($SiMe_3$)$_2$** the *meso* proton is observed at 10.19 ppm; on complexation this shifts to 9.92 ppm, that is, a change of 0.27 ppm which can be attributed to three factors: (a) a shift induced by the bound **BiPy**, (b) a shift induced by the neighbouring porphyrin when the conformation is fixed as a gable and (c) an increased porphyrin-induced ring-current shift resulting from the two porphyrins of the linear dimer being pulled together to a more parallel geometry (less than 60° between porphyrin planes). The degree to which **Zn_2-l-Dim1b($SiMe_3$)$_2$·BiPy** adopts a similar conformation to the cyclic dimer can be estimated from the third chemical shift change listed above, that is the change in chemical shift of the *meso* proton as the angle between the two porphyrins is reduced from 60° in the gable dimer to 0° in the cyclic dimer. An estimate of this change in *meso* chemical shift due to reduction of the 60° gable angle is obtained by comparing the *meso* proton chemical shift of linear dimer when it is bound to **BiPy** (9.92 ppm) and when it is bound to **Py_2Py** (9.98 ppm) Fig. 3(*c*). The difference between these values can be attributed to the influence of the ring current of the second porphyrin as it is pulled closer to the first by the binding of **BiPy**. This interpretation of these values must be treated with caution since the different ligands will induce different changes in the *meso* proton chemical shift depending on the nature of their ring currents, although the differences between **BiPy** and **Py_2Py** are likely to be small. It appears that linear dimer adopts a conformation similar to cyclic dimer when it is bound to **BiPy**, with the two porphyrins held parallel and the alkyne ends in close proximity.

When linear dimer is bound to **H_2-Py_4P** the *meso* protons of the dimer appear at 10.13 ppm. **H_2-Py_4P** forces the porphyrins of linear dimer to be more than 60° apart, thus the *meso* signal is less upfield shifted; this is compounded by the downfield ring current shift of the bound ligand. When half an equivalent of **H_2-Py_4P** was added to linear dimer, then the NH protons in the centre of the ligand cavity resonated at −4.65 ppm, very similar to the shift observed in the cyclic tetramer **H_2-Py_4P** complex (−4.8 ppm; see below), implying that each **H_2-Py_4P** is bound to two linear dimer molecules. If approximately 1 equivalent of **H_2-Py_4P** is added then the ligand signals become broader and a broad NH signal is observed at −3.8 ppm, presumably due to the formation of the 1 : 1 complex. It seems that in contrast to **BiPy** both **Py_2Py** [Fig. 3(*c*)] and **H_2-Py_4P** force the two ends of linear dimer apart.

A competition experiment between the hosts cyclic dimer and linear dimer for **BiPy** was carried out to test the relative affinities of the two hosts for **BiPy**: a ten-fold excess of linear dimer was added to a solution of the recrystallised 1 : 1 **Zn_2-c-Dim1b·BiPy** complex in CD_2Cl_2. By ^{1}H NMR spectroscopy it was possible to distinguish both free and bound signals from linear and cyclic dimer. Integration of the relevant peaks showed that cyclic dimer binds **BiPy** between 100 and 200 times more strongly than linear dimer. Competition experiments between strong binding hosts were very successful, since it is possible to assume that at any given time all the ligand is bound to one or other of the hosts, the ligand distribution ratio being dependent on the relative binding constants. The calculated chelation factors or thermodynamic effective molarities for these processes are shown in Table 2. The difference between the two EMs can be easily rationalised: cyclic dimer has a relatively rigid preformed cavity which is complementary to the **BiPy** ligand, whereas linear dimer freely rotates around the central butadiyne, spending on average only a small proportion of its time in a conformation in which the two porphyrins adopt similar positions to those observed in cyclic dimer. Therefore, significantly more entropy loss accompanies **BiPy** binding to linear dimer than the corresponding binding to cyclic dimer. In the next paper we shall see that **BiPy** is an effective cyclisation template for linear dimer during Glaser–Hay coupling.[2]

Binding properties of the cyclic trimers

As in the case of cyclic dimer **Zn_3-c-Tri1a/b** and **Zn_2H_2-c-Tri1a** have more than one binding site. Their binding curves with pyridine were once again analysed in terms of just three parameters; a single binding constant and two absorption coefficients (for fully bound and fully unbound host). This shows that each binding site is behaving independently. In the case of **Zn_3-c-Tri1b** non-cooperative binding was confirmed by linear Hill plots[24] of unit gradient.§ As with cyclic dimer the empirical binding constants are identical, within experimental error, to those of the corresponding monomers **Zn-Mon1a/b** indicating that there is no hindrance to binding inside the cavities of these host.

Binding curves (from UV–VIS binding data) for co-ordination of the bidentate ligands to **Zn_3-c-Tri1a/b** are biphasic, as reported previously.[6] At low ligand concentrations one ligand molecule binds across two zinc atoms with binding constant K_1, and at higher ligand concentrations a second ligand molecule binds to the third zinc site with binding constant K_2. Only the first binding process is observed with **Zn_2H_2-c-Tri1a** and the K_2 values of **Zn_3-c-Tri1a/b** are very similar to the binding constants of the corresponding monomers **Zn-Mon1a/b**, which provides strong support for this interpretation.

The K_1 value of *ca.* 10^5 for **BiPy** binding to the cyclic trimers is much greater than the 10^3 characteristic of a single binding contact, but model building demonstrates that considerable host distortion is required to allow simultaneous two-point binding. The energetic cost of this distortion is reflected in the value of K_1, which is low for two-point binding. However, this shows that the trimers are elastic hosts, able to respond geometrically to the demands of ligand binding. The K_1 values increase in the series **BiPy**, **Py_2Et**, **Py_2Pr** as the ligands become longer and more complementary to the size of the relaxed trimer cavity. The effective molarity for binding of **Py_2Py** (11–21 mol dm^{-3}) is only slightly greater than that for **Py_2Pr** (5–12 mol dm^{-3}) despite the fact that both ligands are about the same size and **Py_2Py** must be more pre-organised for binding; perhaps there is an unfavourable interaction between the **Py_2Py** phenyl group and the third, unbound porphyrin.

The **Py_3T** ligand attracted our attention because of its good apparent size and shape complementarity with the cavity of the trimeric hosts. As expected, **Py_3T** binds extremely strongly to **Zn_3-c-Tri1a/b** and **Zn_2H_2-c-Tri1a**. The chelation factor of the **Zn_2H_2-c-Tri1a·Py_3T** complex (30 mol dm^{-3}), is slightly larger than that of the **Zn_3-c-Tri1a·Py_2Py** complex (11 mol dm^{-3}), which has a similar coordination geometry but it is only a bidentate ligand. This may reflect the fact that the donor sites are *ca.* 0.2 Å closer together in **Py_2Py** than in **Py_3T**. The formation constant of the **Zn_3-c-Tri1a·Py_3T** complex is high so the measured binding constant is approximate. The titration data are shown in Fig. 2. The information content of this data set is best appreciated by looking at a variance *vs.* K plot such as that shown in Fig. 4.

Such curves are calculated by fitting the experimental data to a range of binding constants; all empirical parameters (such as host concentration and extinction coefficients) are adjusted to minimise the variance between the experimental points and the calculated curve for each value of K. These minimised variances are standardised by dividing by the variance for optimum K, then plotted against K. When K^{-1} > the host concentration, [M] these plots normally give sharp minima, indicating a narrow range of possible K values. However when K^{-1} < [M]

§ Ligands capable of hydrogen bonding to each other within the cavity, such as 4-hydroxymethylpyridine, do show cooperative binding behaviour (L. G. Mackay, E. G. Levy and J. K. M. S., unpublished results).

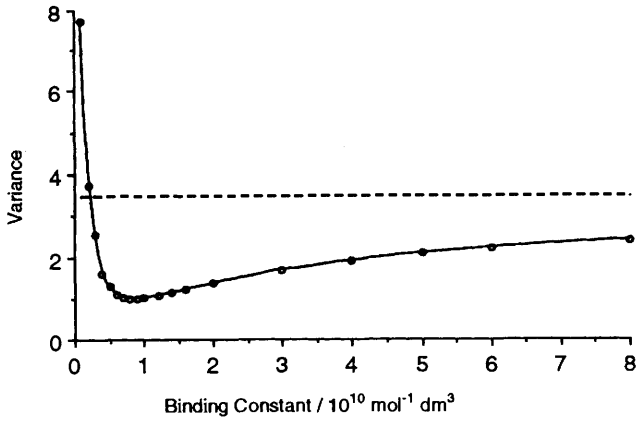

Fig. 4 Variance *vs.* K plot for binding **Py_3T** to **Zn_3-c-Tri1a**. Dashed line shows variance for infinite K.

variance *vs.* K plots become highly unsymmetrical, as seen in Fig. 4; there is a well defined lower limit to K ($\sim 4 \times 10^9$ mol^{-1} dm^3 for **Zn_3-c-Tri1a·Py_3T**), but the variance levels out towards high K. In this case the variance for $K = \infty$ is only 4 times greater than that at the minimum ($K = 9 \times 10^9$ mol^{-1} dm^3), so although the data set is most compatible with a binding constant of 9×10^9 it is only slightly less compatible with much higher values. Fortunately, an upper limit to this binding constant of *ca.* 10^{10} mol^{-1} dm^3 can be obtained from the ^1H NMR experiments described later in this section, so we are confident that the value lies in the range 4×10^9–5×10^{10} mol^{-1} dm^3. Thus, the overall chelation factor or effective molarity of the **Zn_3-c-Tri1a·Py_3T** complex is in the range 1–5 mol dm^{-3}. The effective molarity for binding to the second site during formation of this complex must be close to that of **Zn_2H_2-c-Tri1a·Py_3T** (30 mol dm^{-3}), so the effective molarity for binding of the third site is 0.1–1.0 mol dm^{-3}. The low overall chelation factor is probably a result of strain associated with coordination of the third site; inspection of models indicates that the N–N distance in **Py_3T** (*ca.* 9.6 Å) is 2–3 Å too small to fit the relaxed cavity, and it must be more difficult for the host to bind misfit-guests at three points rather than just two.¶

The ^1H NMR spectrum of **Zn_3-c-Tri1a,b** becomes very broad when **BiPy** is added; the system is in intermediate exchange at room temperature. With **Py_2Et** sharp signals are seen for the bound ligand until almost 1 equivalent of ligand has been added. With **Py_2Pr** and **Py_2Py** the system is in slow exchange until more than 1 equivalent of ligand has been added. Separate signals are seen for free and bound host, but only one set of porphyrin signals is seen for the **Zn_3-c-Tri1a/b**·L complex because intramolecular ligand exchange is fast on the ^1H NMR timescale; the guest rapidly walks round the inside of the cavity. Intermolecular exchange becomes faster when there is more than 1 equivalent of ligand because a singly-bound ligand at the third site is well positioned to substitute the ligand chelated across the other two sites and because ligand exchange can occur by an associative S_N2-like mechanism *via* a six-coordinate zinc intermediate.[13]

The ring-current induced shifts for these ligand–trimer complexes are shown in Figs. 5 and 6. Those of **Py_2Py** (Fig. 5) are particularly informative: the terminal proton of **Py_2Py** experiences an unusually large ring-current because it is forced into close proximity with the third unbound porphyrin.

¶ This interpretation is supported by the **Py_3T**-binding properties of trimers with shorter linkers between the porphyrins: in NMR competition experiments, **Py_3T** is preferentially bound within these smaller cavities where strain-free three-point binding is possible, rather than in the larger cavity of **Zn_3-c-Tri1b**. (A. Vidal-Ferran, N. Bampos and J. K. M. S., unpublished results).

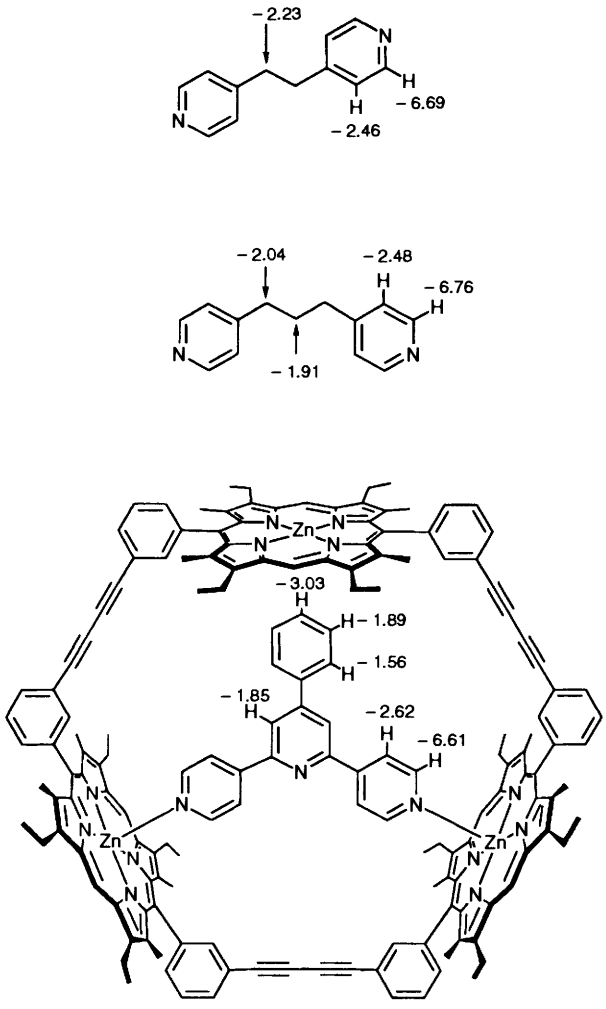

Fig. 5 Changes in ^{1}H NMR chemical shifts on formation of the complexes between **Zn_3-c-Tri1a** and the ligands **Py_2Py**, **Py_2Et** and **Py_2Pr**

Fig. 6 Ring current induced shifts in the **Py_3T·Zn_3-c-Tri1a** complex

The **Zn_3-c-Tri1a,b·Py_3T** complexes are in slow exchange on the NMR time-scale with excess of either component at room temperature. Some of the chemical-shift changes on complexation are marked on Fig. 6. The ring-current shifts of the α- and β-pyridine protons show that all three pyridines bind simultaneously. The internal aromatic proton of the host

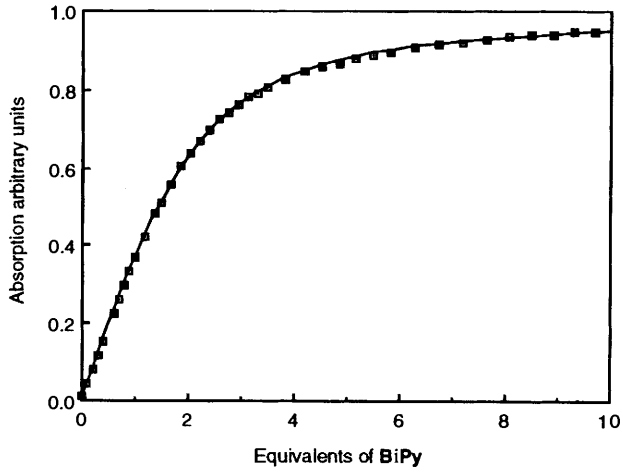

Fig. 7 UV binding curve for titration of **Zn_4-c-Tet1b** with **BiPy** showing experimental points and the theoretical curve for a binding constant of $K = 2 \times 10^8$ mol^{-3} dm

experiences a large downfield shift due to the ring-current of the guest, showing that the pyridyl groups must lie flat in the plane of the three zinc atoms. Molecular mechanics calculations also indicate that **Py_3T** prefers to adopt a planar conformation, which may explain its extremely low solubility.

The free and bound host signals in the ^{1}H NMR spectrum from a 1:1 mixture of **Py_3T·Zn_3-c-Tri1a** and **Zn_3-c-Tri1a**, in $C_2D_2Cl_4$, are seen to coalesce at around 366 K at 400 MHz; analysis of the coalescence temperatures of all the exchanging signals shows that the interconversion rate is 220 s^{-1} at 366 K. The rate limiting step for exchange must be dissociation of the complex, so 220 s^{-1} is also the rate constant for dissociation. This enables one to estimate an upper limit to the binding constant: the rate constant for association cannot exceed the diffusion-controlled limit, which is unlikely to be greater than 10^9 mol^{-1} dm^3 s^{-1}. The ratio of this maximum on-rate to the measured off-rate gives an upper limit to the binding constant of *ca.* 5×10^6 mol^{-1} dm^3 at 366 K. The entropy of binding is unlikely to be greater than *ca.* 130 J mol^{-1} K^{-1} (see later[12]), which corresponds to an upper limit to the binding constant at 300 K of 5×10^9 mol^{-1} dm^3 in $C_2D_2Cl_4$. The binding constant may be higher than this in CH_2Cl_2,[13] but is unlikely to exceed *ca.* 10^{10} mol^{-1} dm^3.

When **Py_3T** is added to a 1:1 mixture of **Zn_3-c-Tri1a** and **Zn_3-c-Tri1b**, signals due to **Py_3T·Zn_3-c-Tri1a** can be distinguished from those of **Py_3T·Zn_3-c-Tri1b** and integration can be used to estimate the relative concentration of the two complexes. This competition experiment showed that the functionalised trimer binds **Py_3T** more strongly by a factor of 4 ± 1. This result is consistent with the binding constants from UV titrations and those described earlier for **Zn-Mon1a,b**.

Binding properties of the cyclic tetramer

CPK models show that the tetramer is the smallest of the butadiyne-linked cyclic oligomers with a strain-free *transoid* arrangement of the aryl linkers; the expected conformational mixture is indeed observed in the NMR spectrum of ligand-free tetramer as described below. The reaction of **BiPy** with **Zn_4-c-Tet1b** to form **Zn_4-c-Tet1b·$(BiPy)_2$** gives isosbestic UV–VIS spectra and a binding curve which fits the calculated isotherm for simple 1:1 binding at twice the real host concentration for $K = 2 \times 10^8$ mol^{-1} dm^3 (as shown in Fig. 7); no significant improvement in the fit was obtained for a two site binding isotherm. This observation is consistent with two interpretations: either (a) binding of the two **BiPy** molecules occurs independently and statistically, and the electronic spectrum of the intermediate 1:1 complex happens to be a linear

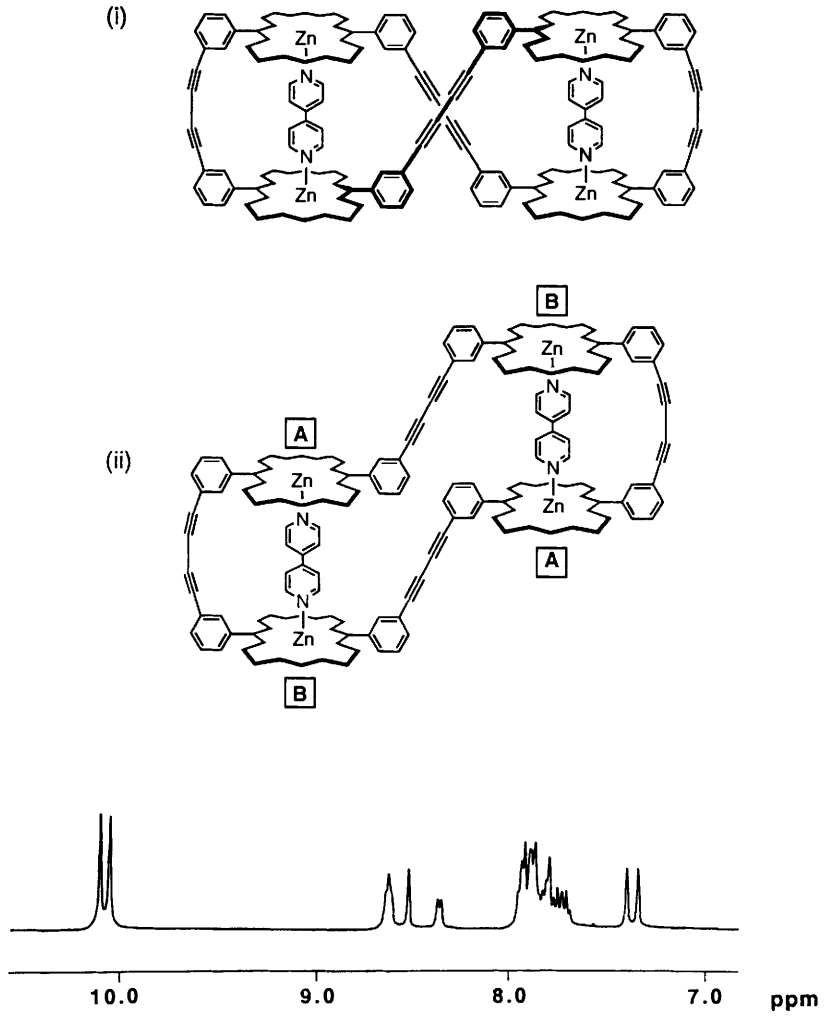

Fig. 8 Proposed structures for the complexes formed between **Zn_4-c-Tet1c** and **BiPip**, and **Zn_4-c-Tet1c** and **BiPy**, and the *meso* and aromatic regions from the ^{1}H NMR spectrum of the **Zn_4-c-Tet1c·(BiPip)$_2$** complex

combination of those of **Zn_4-c-Tet1b** and **Zn_4-c-Tet1b·(BiPy)$_2$** or (b) binding of the two ligands shows strong positive cooperativity, so no significant amount of the 1:1 **Zn_4-c-Tet1b·BiPy** complex is formed. The ^{1}H NMR results discussed below support the latter interpretation. The value of K_1K_2 of 4×10^{16} mol^{-2} dm^6 from the UV titration is close to that determined by ^{1}H NMR competition experiment between cyclic dimer and cyclic tetramer (3×10^{15} mol^{-2} dm^6). This competition experiment and the following ^{1}H NMR titrations were carried out on the solubilised cyclic tetramer, where the methyl esters have been exchanged for isodecyl esters.[10,25] This change in side chain had no detectable effect on the strength of binding but greatly increased the solubility of **Zn_4-c-Tet1b** in deuteriodichloromethane.

The chosen ligand was titrated into a solution of **Zn_4-c-Tet1c** in deuteriodichloromethane and an ^{1}H NMR spectrum was acquired after each addition. This experiment was initially carried out using **BiPy** as the bidentate ligand and then repeated using 4,4′-bipiperidine (**BiPip**). The ^{1}H NMR spectra showed that the complexes formed possessed the same symmetry for both ligands and in both cases integration showed that a 1:2 complex formed. The titration also showed that a single complex was formed both in the presence of excess of guest and in the presence of excess of host. The formation of a single complex over a wide concentration range indicated that there is considerable cooperativity between the addition of the first and the second ligand. The binding of one bidentate ligand sets up the second binding site so that it is more complementary to a second bidentate ligand; the binding constant for the second binding process must be greater than that for the first, so that the 1:1 complex is not formed in detectable concentrations.

The following discussion refers only to the complex formed between **BiPip** and cyclic tetramer **Zn_4-c-Tet1c** which was studied in most detail. Fig. 8 shows the structures which one might expect to be the most probable for a 1:2 complex between cyclic tetramer and **BiPip**. CPK models of these structures seem unstrained and capable of showing cooperative binding. In (i), which has D_2 symmetry, all the porphyrins are *cisoid*, whereas in (ii) which has C_{2h}-symmetry, two are *cisoid* and two *transoid*. The different symmetries lead to distinct differences in the predicted ^{1}H NMR spectra for the complexes.

In the D_2 complex, all four porphyrin environments are the same but the two *meso* environments on each porphyrin are different. When a ligand binds between two of these porphyrins the two ends of the bidentate ligand are in the same environment. In addition, there are two different environments for the phenyl groups. In contrast, the symmetry of the C_{2h} complex gives four different environments for the phenyl groups and two porphyrin environments (A and B). When a ligand binds between two of these porphyrins the two ends of the bidentate ligand are in different environments.

Fig. 8 shows the aromatic and the *meso* regions and Fig. 9 the ligand signals from the ^{1}H NMR spectrum of the recrystallised 1:2 complex formed between cyclic tetramer **Zn_4-c-Tet1c** and

Table 3 Chemical shifts (ppm) of protons *ortho* to the porphyrins and the butadiyne-links. $\Delta\delta$ values are relative to **Zn-Mon1b**. H_2 and H_6 are the *ortho* singlet and doublet protons respectively

Porphyrin	H_2	$\Delta\delta$	H_6	$\Delta\delta$
Zn-Mon1b	8.15	0	8.02	0
Zn_2-c-Dim1c	7.01	−1.14	8.54	0.52
Zn_2-c-Dim1c·BiPip	6.51	−1.64	8.75	0.73
Zn_2-c-Dim1c·BiPy	6.32	−1.83	8.73	0.71
Zn_4-c-Tet1c (BiPip)$_2$	7.24, 7.30, 7.68, 8.40	−0.91, −0.85, −0.47, 0.25	8.54, 8.52, 8.25, 7.72	0.52, 0.50, 0.23, −0.30
Zn_2-c-Tet1c (BiPy)$_2$	7.26, 7.31, 7.68, 8.46	−0.89, −0.84, −0.47, 0.31	8.56, 8.56, 8.33, 7.74	0.54, 0.54, 0.31, −0.28
Zn_3-c-Tri1b	8.06	−0.09	7.99	−0.03

BiPip. The experimentally observed pattern of two equal intensity *meso* singlets is consistent with either symmetry, and is therefore not diagnostic. The bound ligand signals appear upfield of TMS due to the effect of the porphyrin ring currents. The NH signals were located with a deuterium oxide shake. As expected, the signals for the NH proton were the most shielded by the porphyrin ring current and appeared at −5.86 and −5.99 ppm as two equal intensity triplets, indicating that the two ends of the **BiPip** ligand are not in the same environment and giving support for structure (ii). Such pronounced splittings were not observed for the other ligand signals since these protons must be too far away from the porphyrins to be strongly influenced by this effect.

The aromatic protons from the phenyl rings form a complex series of multiplets. However, it was possible to discern in a ^{1}H–^{1}H COSY spectrum (not shown) four separate sets of four-proton aromatic signals, again favouring structure (ii); the four apparent singlets corresponding to the isolated proton between the porphyrin and alkyne linkages are marked $H_{21,\ II,\ III,\ IV}$ in Fig. 9.‖ It was not possible to assign each spin system unambiguously, but ring current-induced changes in chemical shifts on complexation were used to assign H_{2I} and H_{2IV}, and to assign the pair of protons H_{2II} and H_{2III}, although not to distinguish between them.

Table 3 gives the chemical shifts of the four apparent *ortho* singlets H_2, along with those for other oligomers and their complexes. The second column shows these chemical shifts relative to monomer. The third column gives the chemical shifts for H_6 signals. When cyclic dimer binds to **BiPip** the H_2 protons are shielded by 0.50 ppm and appear at 6.51 ppm, whilst their H_6 partners are deshielded and shifted in the opposite direction to 8.75 ppm. The H_2 resonances in the cyclic dimer **BiPy** complex are shifted upfield relative to those in the **BiPip** complex, suggesting that the **BiPy** ring current also has an effect.

Upfield shifted H_2 protons have a downfield shifted H_6 partner. Two of the H_2 protons of the cyclic tetramer **BiPip** complex are shielded relative to the other two and appear at 7.24 and 7.30 ppm, and their H_6 partners at 8.52 and 8.54 ppm. This suggests that these signals are from the two protons in the most cyclic dimer-like environments, H_{2II} and H_{2III}, leaving H_{2IV} and H_{2I} to be the signals at 7.68 and 8.4 ppm. The shielded nature of the two protons H_{2II} and H_{2III} also rules out the formation of a 2:4 complex in which the **BiPip** binds between two molecules of cyclic tetramer. If this were the case then it would be unlikely that the two adjacent porphyrins of the cyclic tetramer would be bent towards one another so as to cause the required shielding. The signal observed at 8.40 ppm can be assigned to H_{2I} because these are the only H_2 protons which move downfield on binding to **BiPip**. The partner H_6 protons are moved upfield to 7.72 ppm by complexation to **BiPip**. These chemical-shift changes are in the opposite direction to those observed for the other three pairs of H_2 and H_6 protons. Since H_{2I} is on the outside of the complex it only experiences the ring current from its own porphyrin, unlike H_{2II} and H_{2IV} which are in a similar environment to that in cyclic dimer and are, therefore, shielded. The most deshielded *ortho* singlet (8.40 ppm) is most likely to be H_{2I}, leaving H_{2IV} to be the signal at 7.68 ppm.

A NOESY spectrum acquired with 300 ms mixing time confirmed the assignment of the H_{2II} H_{2III} protons and assigned the bound **BiPip** protons as summarised in Fig. 9. The symmetry of the proposed structure was further supported by ^{13}C NMR (partially assigned by C–H *J*-modulation). This spectrum showed that there were eight alkyne carbons from the butadiyne links and two C–H *meso* environments as expected. The alternative structure (i) would only give four alkyne carbon environments.

Cyclic porphyrin tetramer **Zn_4-c-Tet1b** binds to tetrapyridyl porphyrin **H_2-Py_4P** with a binding constant of 2×10^{10} $mol^{-1}dm^3$ (see Fig. 10). Usually it is not possible by UV–visible spectroscopy to measure binding constants of this magnitude directly, but in this case, measurement was facilitated by the very large extinction coefficient ($2 \times 10^6 \cdot cm^{-1}mol^{-1}dm^3$) at λ_{max} for cyclic porphyrin tetramer (**Zn_4-c-Tet1b**). The ligand absorbs strongly in the same region of the UV spectrum as the host but this proved to be no disadvantage when determining binding constants, since once the extinction coefficient for **H_2-Py_4P** at the wavelengths in question have been measured then the ligand concentration can be checked after each addition.

The NMR spectrum of ligand-free tetramer confirms that the molecule exists in several conformations which are in slow exchange on the chemical shift timescale;[8] one possible conformer is shown schematically in Fig. 11. Aryl ring rotation is in slow exchange at room temperature for the zinc monomer, and might be expected to be even slower in a cyclic oligomer. When **H_2-Py_4P** is added to a solution of **Zn_4-c-Tet1b** a strong 1:1 complex forms which is in slow exchange with excess of guest on the ^{1}H NMR chemical-shift timescale and chromatographs on silica as a single band. Once **H_2-Py_4P** is bound it prevents the porphyrin units in cyclic tetramer from undergoing *cis–trans* interconversion and favours a more symmetrical conformation. Since the ester methyl (Me_a) and the ring methyl (Me_b) signals each give rise to two equal intensity singlets separated by 0.28 and 0.05 ppm respectively, we can rule out the D_{4h} conformation shown schematically in Fig. 11. Similar splittings are also observed in the ^{13}C NMR. Molecular mechanics calculations and CPK models indicate the complex **H_2-Py_4P·Zn_4-c-Tet1b** prefers to adopt a tub-shaped geometry reminiscent of cyclooctatetraene (Fig. 12). The D_{2d} symmetry is consistent with the split signals observed in the ^{1}H and ^{13}C NMR. These splittings result from the presence of the two pyrrole environments (Fig. 12); the axial pyrroles are shaded black.

The α- and β-pyridine protons of **H_2-Py_4P** in the complex

‖ Strong cross-peaks due to W-coupling over four bonds were observed in the COSY spectrum.

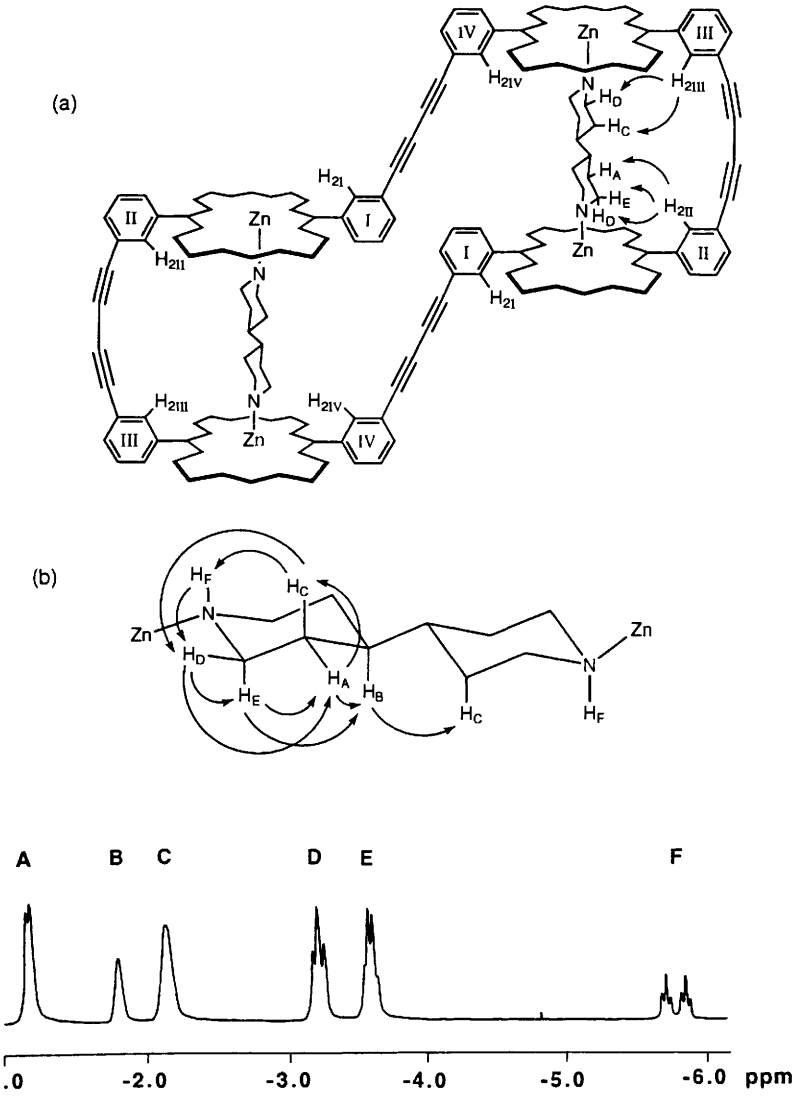

Fig. 9 (*a*) NOEs observed between **Zn_4-c-Tet1c** and **BiPip**. (*b*) NOEs observed within the bound ligand and the assignment of the one dimensional ^{1}H NMR spectrum for the bound **BiPip** signals.

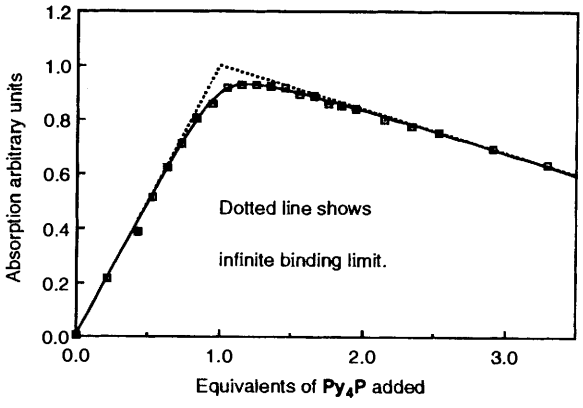

Fig. 10 UV–visible binding curve for the titration of **Zn_4-c-Tet1b** with **H_4Py_4P**. Experimental points on the theoretical curve for $K = 2 \times 10^{10}$ mol^{-3} dm.

appear as sharp doublets at 2.26 ppm and 5.77 ppm, respectively. The α-pyridine protons of **H_2-Py_4P** are shifted upfield by 6.81 ppm and the β-protons by 2.41 ppm on complexation to cyclic tetramer. When these upfield shifts are compared with those observed in other pyridine–zinc porphyrin complexes it is clear that all four porphyrins must be bound simultaneously. The NH signal of the **H_2-Py_4P** is shifted by 2.9 ppm upfield to −4.8 ppm. This upfield shift is consistent with four porphyrin ring-currents perpendicular to the ligand plane and in close proximity.** A similar geometry is observed for the **Zn-Py_4P·Zn_4-c-Tet1b** complex in solution.

An estimate of the relative values of the binding constants for the complexes formed between cyclic tetramer **Zn_4-c-Tet1b** **BiPy**, **BiPip** and **H_2-Py_4P** was obtained from a ^{1}H NMR competition experiment. At millimolar concentrations the order of stability for the three complexes was **BiPip** > **BiPy** > **H_2-Py_4P**. More quantitative experiments between ligands were unsuccessful since a small proportion of the free ligand reacted with the solvent deuteriodichloromethane during the acquisition of ^{1}H NMR spectra. This was a particular problem with the more nucleophilic **BiPip**.

Binding properties of the linear tetramer

BiPy binds to linear tetramer **Zn_4-1-Tet1b($SiMe_3$)$_2$** with an affinity of 7×10^6 mol^{-1} dm^3; the UV–VIS data were analysed for a simple statistical 1:1 binding process and the simulated curve was found to fit the experimental data very well,

** The symmetry of the complex in the crystal structure is essentially identical with that observed in solution.[26]

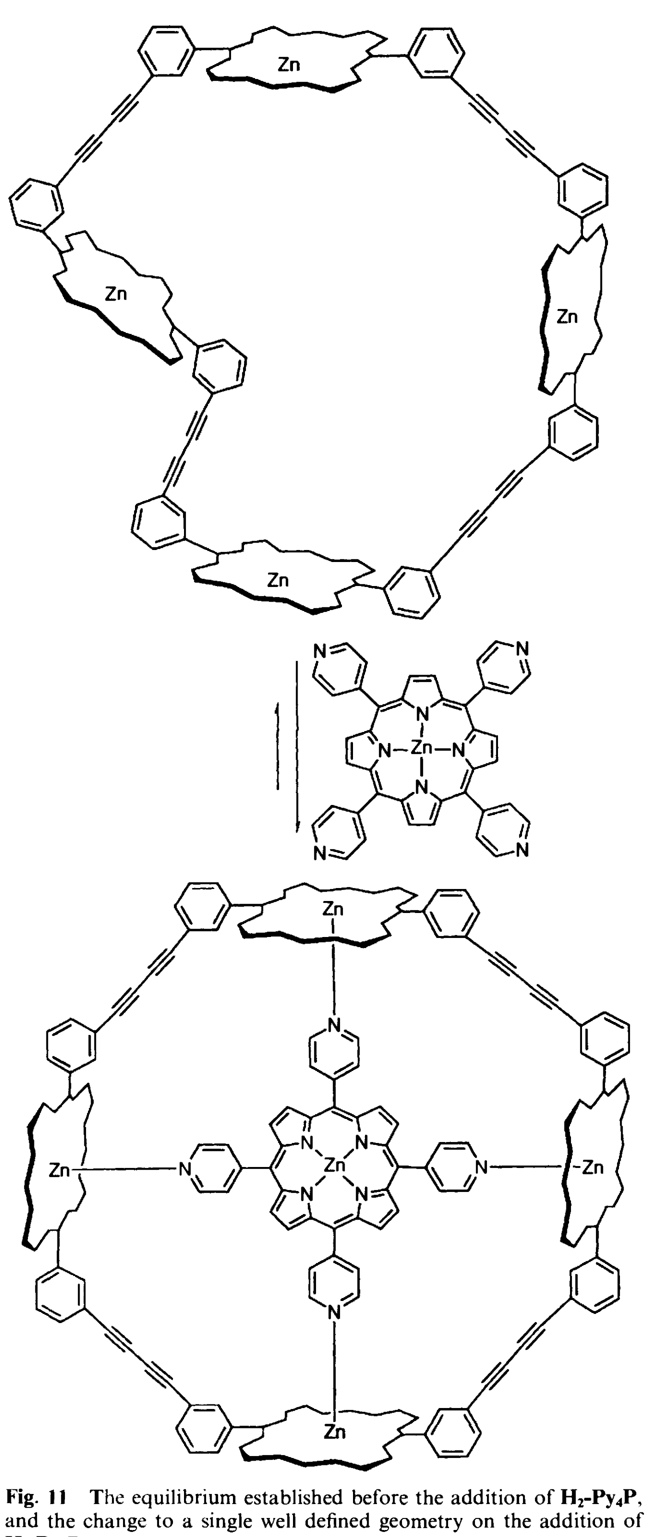

Fig. 11 The equilibrium established before the addition of H_2-Py_4P, and the change to a single well defined geometry on the addition of H_2-Py_4P

indicating that the two binding events are either completely statistical or cooperative. Insights into the structure of the linear porphyrin pyridyl complexes are obtained from the template-directed cyclisation experiments described in the following paper.[2]

Linear tetramer **Zn_4-l-Tet1b($SiMe_3$)$_2$** may form 1:1 or 1:2 complexes with **H_2-Py_4P** depending on the concentration of linear tetramer and **H_2-Py_4P**. The relative stability of these species will determine the best concentration at which to measure the binding constant for the 1:1 complex. The 1:1 complex will be favoured at low concentrations. The experimental data from the titration are shown in Fig. 13 along with the simulated curve for simple 1:1 binding with a binding constant of 7×10^9 mol^{-1} dm^3. The good fit indicates that at this concentration the predominant species being formed is the 1:1 complex between linear tetramer and **H_2-Py_4P**. The binding constant is very similar to, but clearly smaller than, that for the complex formed between cyclic tetramer and **H_2-Py_4P** (2×10^{10} mol^{-1} dm^3). This difference was qualitatively confirmed by an NMR competition experiment for **H_2-Py_4P** between linear **Zn_4-l-Tet1b($SiMe_3$)$_2$** and cyclic tetramer **Zn_4-c-Tet1b**.

H_2-Py_4P was titrated into a solution of **Zn_4-l-Tet1b($SiMe_3$)$_2$** (4 mmol dm^{-3}) in deuteriochloroform, and after each addition a ^{1}H NMR spectrum was recorded. As **H_2-Py_4P** was added to linear tetramer the singlet TMS signal split, showing the existence of several different environments. Up to the addition of 1 equivalent of **H_2-Py_4P** the NH signal from the **H_2-Py_4P** was observed at -4.7 ppm, a very similar shift to the -4.8 ppm observed for the complex with cyclic tetramer. Similarly, the β-pyridine signal for the ligand (5.77 ppm) which appears as a broad singlet has approximately the same chemical shift as the analogous protons in the cyclic tetramer **H_2-Py_4P** complex. This can be rationalised by the formation of a 1:1 complex in which the linear tetramer wraps itself around the central **H_2-Py_4P**, which would account for the similar changes in chemical shift on complexation compared with those observed for the cyclic tetramer **H_2-Py_4P** complex. The presence of several TMS proton environments could be consistent with the formation of the 1:1 complex since rotation about the porphyrin-aryl bond is slow on the ^{1}H NMR time-scale.

When more than 1 equivalent of **H_2-Py_4P** was added the TMS proton pattern changed completely to give a new set of signals, the β-pyridine signals became broad and disappeared and the NH proton was observed at -3.1 ppm. This is consistent with the formation of a greater proportion of a 1:2 [**Zn_4-l-Tet1b($SiMe_3$)$_2$:2H_2-Py_4P**] complex as the ligand concentration is increased. From ^{1}H NMR spectra of a 1:1 mixture of linear tetramer and **H_2-Py_4P** over the concentration range 4 to 0.1 mmol dm^{-3} there is little evidence for the formation of higher order aggregates, so it seems that at millimolar concentrations the 1:1 complex between linear tetramer and **H_2-Py_4P** is probably most favourable.

We have been unable to elucidate fully the structure of the complexes formed between linear tetramer and **H_2-Py_4P**. However, it is important to note that the type of complex observed is dependent on the concentration of the host and the guest as this has implications for the template-directed reactions described in the two following papers.[2]

The binding of **BiPy** and **BiPip** to the linear tetramer was also explored. In both cases up to the addition of 2 equivalents of ligand a complex formed which was in slow exchange on the ^{1}H NMR timescale. The ^{1}H NMR spectrum was very complicated and had a large number of signals corresponding to TMS protons. This can be accounted for again by slow rotation about the aryl–porphyrin bond on the ^{1}H NMR time-scale, and the presence of more than one complex.

Conclusions

The ligand-binding properties of the cyclic dimer and trimer show that they are pre-organised in open conformations, even in the absence of guests, and they must have cavities which are so spacious that one ligand can bind on the inside without hindering other ligands from also binding on the inside. A recent crystal structure[27] and catalytic results[4,5] have confirmed that indeed two or more ligands can be bound independently within the cavity.

Binding constants up to 10^{10} mol^{-1} dm^3 were measured by

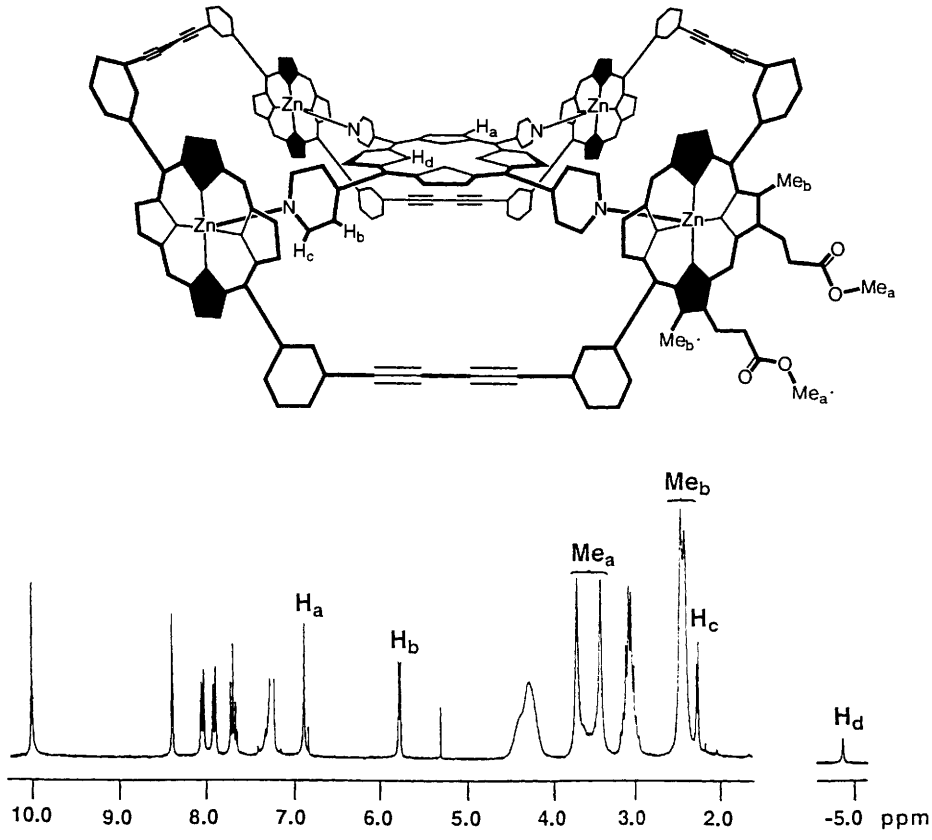

Fig. 12 Structure and ^{1}H NMR of the **Zn_4-c-Tet1b·H_2-Py_4P** complex

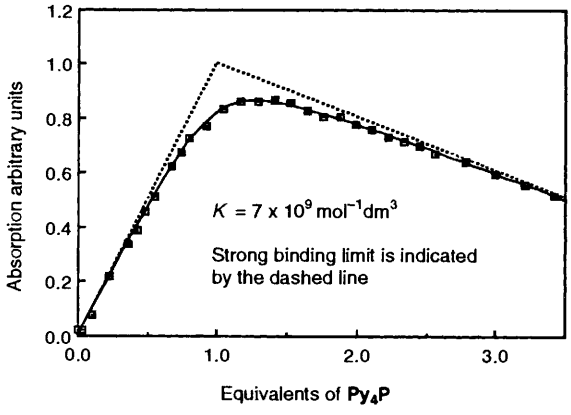

Fig. 13 UV–VIS binding curve for titration of **Zn_4-1-Tet1b($SiMe_3$)$_2$** with **H_2-Py_4P** showing the experimental points and the theoretical curve

monitoring changes in the UV–VIS spectra of the porphyrin oligomers as a function of the added ligand concentration, and by ^{1}H NMR analysis of mixtures of hosts competing for a given ligand. The latter approach was particularly useful for checking the consistency of binding constants measured by UV–VIS titration.

Both the cyclic dimers **Zn_2-c-Dim1b,c** and the cyclic trimers **Zn_3-c-Tri1a,b** exhibit effective molarities in the range 10–100 mol dm^{-3} when binding complementary bidentate ligands. Such ligands are transition-state analogues for reaction of monodentate substrates, so it should be possible to translate thermodynamic chelation factors into kinetic effective molarities and rate enhancements of 10^4–10^5 at 1 mmol dm^{-3} concentrations by looking at transfer reactions such as that illustrated in Fig. 1(*b*) of the preceding paper.[1] Although the effective molarities exhibited by these systems are higher than those of other porphyrin dimer complexes, they are several orders of magnitude lower than those reported for intramolecular reaction in small molecules and those for enzyme–inhibitor binding.[28] Calculations indicate that this is likely to be an intrinsic property of the weak and flexible Zn–N bond.

The very large binding constants and effective molarities exhibited by the **BiPy·Zn_2-c-Dim1b,c** and **Py_3T·Zn_3-c-Tri1a,b** complexes are consistent with fast association rates that approach diffusion controlled. This is further evidence that the cavities are open and accessible, although they must be solvent filled. The distinctive feature of these hosts is that they are not floppy, but nor are they completely rigid. They are conformationally homogeneous, yet are able to flex in response to chelating ligands covering a range of sizes; it may be that this responsiveness to ligand geometry is a key feature of the trimer's success as a catalyst.

The cyclic tetramer is a more flexible host. It can adopt several very different conformations, and is thus able to bind to a diverse range of guests, even when they have no obvious complementarity to its cavity.†† Linear tetramer **Zn_4-1-Tet1b($SiMe_3$)$_2$** binds to **H_2-Py_4P** less strongly than cyclic tetramer **Zn_4-c-Tet1b** but only by a factor of *ca.* 10. In other words, there is not as much advantage to be gained, in binding energy terms, by joining the two ends of linear tetramer to form cyclic tetramer, as we saw for linear and cyclic dimers. The values given in Table 2 correspond to EM for binding of two adjacent porphyrins of linear tetramer once two of the four porphyrins have bound to **H_2-Py_4P**. The binding constant for

†† Hydrogenation of the butadiyne linkers of **Zn_3-c-Tri1b** gives a conformationally heterogeneous tetramethylene-linked host that exhibits even more complicated responses to structurally diverse ligands (N. Bampos, V. Marvaud and J. K. M. S., unpublished results).

two adjacent porphyrin units of linear tetramer binding to **H_2-Py_4P** can be assumed to be very similar to that observed for linear dimer and **H_2-Py_4P**, that is 3×10^6 mol^{-1} dm^3. The binding equilibria are much more complicated for the linear hosts because of the greater number of conformations they can adopt. These two factors—the lower chelate factors and the greater flexibility—both favour the formation of a range of complexes with different stoichiometries. The cyclic trimer has already demonstrated important catalytic activity[4,5] while the potential of the other linear and cyclic oligomers as model enzymes has yet to be explored.

Experimental

All ^{1}H NMR spectra were recorded on Bruker AM-400 or Bruker WM-250 spectrometers, in $CDCl_3$, except for high temperature spectra which were recorded in $C_2D_2Cl_4$. UV spectra were recorded on a Pye Unicam PU 8800 and Perkin Lambda 2 spectrophotometers.

4′-Phenyl-4,2′:6′,4″-terpyridyl (Py_2Py)[16,17]

Boron trifluoride–diethyl ether (17 cm^3, 135 mmol) was added dropwise to benzaldehyde (2.5 cm^3, 25 mmol) and 4-acetylpyridine (6 cm^3, 54 mmol) and the mixture was stirred at 100 °C for 6 h. Acetic acid (25 cm^3) and ammonium acetate (20 g) were added to the mixture which was then heated at 100 °C for a further 8 h to give a tarry solid mass. This was dissolved in dilute hydrochloric acid (500 cm^3) and the solution neutralised to pH 9 with sodium hydroxide and extracted with chloroform (200 cm^3). Evaporation of the extract gave a brown tar which revealed white crystals when washed with methanol (100 cm^3). This mixture of **Py_2Py** and 2′-phenyl-4,4′:6′,4″-terpyridyl was separated by flash chromatography, eluting with 5% methanol in ethyl acetate. The first band yielded **Py_2Py** (450 mg, 6%), mp 283–284 °C; δ_H(250 MHz, $CDCl_3$) 7.75 (3 H, m), 7.74 (2 H, d), 8.04 (2 H, s), 8.79 (4 H, d) and 8.79 (4 H, d); *m/z* 309 (M^+) (Found: C, 81.6; H, 4.7; N, 13.6. $C_{21}H_{15}N_3$ requires C, 81.53; H, 4.89; N, 13.58%).

The second band yielded 2′-phenyl-4,4′:6′,4″-terpyridyl (350 mg, 5%) mp 264–265 °C; δ_H(250 MHz, $CDCl_3$) 7.73 (3 H, m), 7.64 (2 H, d), 7.94 (1 H, s), 7.98 (1 H, s), 8.12 (2 H, d), 8.19 (2 H, d), 8.78 (2 H, d) and 8.80 (2 H, d); *m/z* 309 (M^+) (Found: C, 81.3; H, 4.7; N, 13.4. $C_{21}H_{15}N_3$ requires C, 81.53; H, 4.89; N, 13.58%).

s-Tri(4-pyridyl)triazine (Py_3T)[17]

A mixture of 4-cyanopyridine (10 g, 96 mmol), 18-crown-6 (1 g, 3.8 mmol), potassium hydroxide (225 mg, 4.0 mmol) and decalin (10 cm^3) was stirred at 200 °C under argon for 3 h and then evaporated to give a brown solid. This was washed with hot pyridine (3×50 cm^3) to leave white crystals, which were dissolved in dilute hydrochloric acid (50 cm^3), reprecipitated with aqueous ammonia, filtered off and dried *in vacuo*; yield 7.4 g (74%). Part of this material when sublimed (220 °C, 0.01 mmHg) remained unchanged (^{1}H NMR or UV); mp > 300 °C; δ_H(250 MHz, $CDCl_3$) 8.56 (6 H, d) and 8.94 (6 H, d); *m/z* 312 (M^+).

Measurement of binding constants by UV–VIS titration

Two solutions were made up in dichloromethane (freshly distilled off CaH_2), both of which had the same zinc porphyrin concentration (10^{-8}–10^{-6} mol dm^{-3}) but one of which also contained a large excess of the ligand (10^{-6}–10^{-2} mol dm^{-3}). An accurately measured volume of the ligand-free solution was placed in an oven-dried 10 mm quartz cuvette and microlitre quantities of the other solution were titrated into it. The Soret band shifted from 409 to 423 nm during pyridine binding. The absorption was monitored at these wavelengths of maximum intensity change and spectra were plotted to check for isosbesticity. Ligand was added in sufficiently small quantities to give *ca.* 30 pairs of readings evenly distributed over the binding curve. Porphyrin concentrations were chosen to give an absorbance of around unity at λ_{max} (*ca.* 10^{-6} mol dm^{-3}), except when strong binding constants were being measured, when concentations 20 times more dilute than this were used.

Each binding constant was measured at least twice. For cyclic dimer and trimer values lower than 10^8 mol^{-1} dm^3 are reproducible to within ±20%, the main factors limiting reproducibility being volume measurement error, evaporation loss during the course of titration and temperature variation. The cell temperature was generally 27 ± 3 °C except where indicated to the contrary (a variation of only 3 °C with ΔS of 100 J K^{-1} mol^{-1} would account for a 5% variation in binding constant). Binding constants become difficult to measure when they are so strong that there is little dissociation, so values greater than 10^8 mol^{-1} dm^3 for dimer and trimer are approximate (±50%) and values greater than 10^9 mol^{-1} dm^3 must be regarded as order of magnitude estimates.

Binding constants of 10^{10} mol dm^{-3} with cyclic tetramer can be measured more accurately than those for trimer because there are four porphyrins in cyclic tetramer. The extinction coefficient for cyclic tetramer allows measurement of binding constants of 10^{10} mol dm^{-3} to within ±50% since titrations can be carried out at lower concentrations. In titrations with **H_2-Py_4P** as the ligand the following extinction coefficients were used: $\varepsilon_{427} - \varepsilon_{412} = -2.16 \times 10^5$ mol^{-1} dm^3 and $\varepsilon_{424} - \varepsilon_{411} = -1.49 \times 10^5$ mol^{-1} dm^3 and absorptions were measured at 412 and 427 nm, these being the wavelengths of maximum intensity change during the titration. Binding constants were extracted from the titration curves using a simplex least-squares curve-fitting program.[18]

Zn_4-c-Tet1c. A mixture of **H_8-c-Tet1b** (43 mg, 12 μmol) and benzyl alcohol (20 cm^3) was thoroughly degassed and saturated with argon. Titanium(IV) tetraisopropoxide (200 mm^3) was added to the mixture which was then stirred at 105 °C, 13 mmHg for 4 h, by which time all the porphyrin was in solution. Solvent was removed from the mixture by evaporation under reduced pressure and the product dried *in vacuo* to remove all traces of the benzyl alcohol. 3,7-Dimethyloctan-1-ol (20 cm^3) was then added to the mixture and the procedure outlined above for the trans-esterification with benzyl alcohol repeated. The intermediate benzyl ester porphyrin was required because **H_8-c-Tet1b** was insufficiently soluble in 3,7-dimethyloctan-1-ol for direct trans-esterification. The benzyl cyclic tetramer was not used directly because the ^{1}H NMR of the benzyl side chains overlapped with the very characteristic aromatic region of the cyclic porphyrin tetramer. After removal of solvent from the mixture the product was dissolved in $CHCl_3$ and passed down a short silica column eluting with $CHCl_3$. Zinc metallation was carried out using the standard procedure and the product was recrystallised from $CHCl_3$–MeOH to yield **Zn_4-c-Tet1c** (68 mg, 97%); R_F 0.17 in $CHCl_3$; δ_H(250 MHz; CD_2Cl_2) 0.33–1.50 (304 H, m), 2.31–2.54 (48 H, m), 2.84–3.15 (32 H, m), 3.67–4.38 (64 H, m), 7.6–8.5 (32 H, m), 10.00, 10.12 and 10.84 (8 H, m); $\lambda_{max}(CH_2Cl_2)$/nm 333, 412, 538 and 574.

Zn_4-c-Tet1c·(BiPy)$_2$. **Zn_4-c-Tet1c** (30 mg, 5.1 μmol) and **BiPy** (6 mg, 38 μmol) were dissolved in CH_2Cl_2 (5 cm^3) after which most of the solvent was removed from the mixture before recrystallisation of the residue from $CHCl_3$–MeOH to yield **Zn_4-c-Tet1c·(BiPy)$_2$** (24.5 mg, 77%) (Found: C, 75.15; H, 8.3; N, 4.4. $C_{388}H_{504}N_{20}O_{32}Zn_4$ requires C, 74.9; H, 8.2; N, 4.5%); δ_H(250 MHz; CD_2Cl_2) 0.71–1.72 (304 H, m), 1.74 (4 H, d), 1.78 (4 H, d), 2.41 (48 H, t), 3.05 (32 H, br m), 4.03–4.29 (64 H, m), 4.69 (8 H, d), 7.25 (2 H, s), 7.31 (2 H, s), 7.68–7.84 (20 H, m), 8.34 (2 H, d), 8.46 (2 H, s), 8.56 (4 H, br d), 10.09 (4 H, s) and 10.05 (4 H, s).

Zn_2-c-Diml c. A mixture of **H_4-c-Diml b** (170 mg, 94 μmol) and benzyl alcohol (20 cm^3) was thoroughly degassed and saturated with argon.

Titanium(IV) tetraisopropoxide (200 mm^3) was added to the mixture which was then heated under reflux at 105 °C, 13 mmHg for 4 h, by which time all the porphyrin had dissolved. The solvent was removed under reduced pressure and the product dried *in vacuo* to remove all traces of the benzyl alcohol. 3,7-Dimethyloctan-1-ol (20 cm^3) was then added to the mixture and the procedure outlined for the trans-esterification with benzyl alcohol repeated. After removal of the solvent from the mixture the product was dissolved in $CHCl_3$ and the solution passed down a short silica column eluting with $CHCl_3$. Zinc metallation was carried out using the standard procedure. The product was recrystallised from $CHCl_3$–MeOH to yield **Zn_2-c-Diml c** (197 mg, 71%); R_F 0.24 in $CHCl_3$ (Found: C, 74.9; H, 8.3; N, 3.7. $C_{184}H_{244}N_8O_{16}Zn_2$ requires C, 74.8; H, 8.3; N, 3.8%); δ_H(400 MHz; CD_2Cl_2) 0.65–1.52 (152 H, m), 2.33 (24 H, s), 2.94 (16 H, m), 3.98–4.22 (32 H, m), 6.99 (4 H, s), 7.72 (8 H, m), 8.54 (4 H, br d) and 9.93 (4 H, s); δ_C(100 MHz; CD_2Cl_2) 15.8, 19.5, 21.9, 22.55, 22.64, 24.7, 28.1, 30.1, 35.7, 37.3, 39.4, 63.3, 65.9, 74.5, 82.7, 97.4, 117.7, 121.4, 127.4, 130.2, 133.4, 138.9, 139.4, 141.9, 143.7, 145.5, 147.3 and 173.0 [Found: *m/z* (MALDITOF) 2955 (M^+). $C_{184}H_{244}N_8O_{16}Zn_2$ requires 2955.12].

Zn_2-c-Diml c·BiPy. Zn_2-c-Diml c (66 mg, 22 μmol) and **BiPy** (10 mg, 64 μmol) were dissolved in CH_2Cl_2 (10 cm^3) after which most of the solvent was removed from the solution before it was layered in methanol; recrystallisation of the product yielded **Zn_2-c-Diml c·BiPy** (62 mg, 91%) (Found: C, 75.05; H, 8.3; N, 4.4. $C_{194}H_{252}N_{10}O_{16}Zn_2$ requires C, 74.9; H, 8.2; N, 4.5%); δ_H(400 MHz; $CDCl_3$) 0.71–1.54 (156 H, m), 2.35 (24 H, s), 2.96 (16 H, t), 4.00 (16 H, m), 4.25 (16 H, m), 4.63 (4 H, d), 6.34 (4 H, s), 7.69 (8 H, m), 8.73 (4 H, d) and 9.85 (4 H, s); δ_C(100 MHz; $CDCl_3$) 16.0, 19.4, 21.8, 22.6, 24.5, 27.9, 29.9, 25.5, 37.1, 37.2, 39.1, 63.2, 73.8, 81.8, 97.3, 116.2, 118.8, 120.7, 126.8, 130.4, 133.2, 138.0, 138.9, 141.6, 142.7, 142.8, 143.6, 145.5, 146.6 and 173.0 [Found: *m/z* (MALDITOF) 2955 (M^+ − BiPy). $C_{194}H_{252}N_{10}O_{16}Zn_2$ requires 3111.0].

Competition between Zn_4-c-Tet1c and Zn_2-c-Diml c for BiPy. Zn_4-c-Tet1c·$(BiPy)_2$ (30 mg, 4.8 μmol) was dissolved in CD_2Cl_2 (400 mm^3) to which portions of a solution of **Zn_2-c-Diml c** (25 mmol dm^{-3} in CD_2Cl_2) were added. After each addition a ^1H NMR spectrum was acquired. Additions were continued until a spectrum showing comparable proportions of **Zn_4-c-Tet1c**, **Zn_2-c-Diml c**, **Zn_2-c-Diml c·BiPy** and **Zn_4-c-Tet1c·$(BiPy)_2$** was obtained. Integration of the relevant peaks allowed the calculation of the relative magnitudes of the two binding constants.

Competition between Zn_2-c-Diml b and Zn_2-c-Diml c for BiPy. Zn_2-c-Diml b (1 mg, 0.5 μmol) and **Zn_2-c-Diml c·BiPy** (1.6 mg, 0.5 μmol) were dissolved in CD_2Cl_2 (400 mm^3). The ^1H NMR spectrum of the sample was recorded with a 3 s relaxation delay. Integration was carried out on the *meso* region and on the *ortho* protons, to determine the proportions of free and bound dimers in the mixture and hence the relative value of the two binding constants.

Zn_4-c-Tet1c·$(BiPip)_2$. The procedure was the same as for the preparation of **Zn_4-c-Tet1c·$(BiPy)_2$** except that **BiPip** (6 mg, 0.36 mmol) was used as the ligand; yield of **Zn_4-c-Tet1c·$(BiPip)_2$** after recrystallisation from $CHCl_3$–MeOH (25.2 mg, 79%); δ_H(400 MHz; CD_2Cl_2) −5.99 (2 H, t), −5.85 (2 H, t), −3.65 (4 H, t), −3.27 (4 H, t), −2.17 (4 H, br s), −1.81 (2 H, br s), −1.14 (4 H, br s), 0.69–1.73 (304 H, m), 2.37–2.47 (48 H, m), 2.94–3.20 (32 H, m), 3.96–4.26 (48 H, m), 4.26–4.56 (32 H, m), 7.24 (2 H, s), 7.30 (2 H, s), 7.60–8.00 (20 H, m), 8.25 (2 H, d), 8.40 (2 H, s), 8.52 (4 H, m), 9.99 (4 H, s), 10.04 (4 H, s); δ_C(100 MHz; CD_2Cl_2) 15.8, 16.0, 19.6, 22.1, 22.6, 22.7, 24.8, 27.2, 28.2, 30.2, 35.8, 37.3, 37.6, 39.4, 40.7, 40.8, 63.3, 74.0, 74.2, 74.3, 81.8, 82.0, 83.0, 97.3, 97.4, 117.3, 117.5, 117.6, 121.0, 121.1, 127.56, 127.64, 127.7, 127.9, 130.4, 130.5, 132.0, 132.4, 133.8, 134.2, 134.4, 137.2, 138.4, 138.6, 138.7, 139.1, 139.3, 141.5, 141.6, 141.7, 141.8, 144.6, 144.7, 145.0, 146.2, 146.2, 147.3, 147.5, 147.7, 173.1 and 173.2.

Zn-Py_4P·Zn_4-c-Tet1b. Zn_4-c-Tet1b (38 mg, 10 μmol) and **Zn-Py_4P** (10 mg, 15 μmol) were dissolved in $CHCl_3$ (75 cm^3). The mixture was degassed, saturated with argon and left under reflux. After 2 h the reaction seemed complete by TLC (this was not easy to determine because some decomplexation occurred on the plate). The solvent was partially evaporated and the porphyrin passed down a short silica column eluting with **Zn-Py_4P** ‡‡-saturated $CHCl_3$. The product was recrystallised from **Zn-Py_4P**-saturated $CHCl_3$ with layering into MeOH to yield **Zn-Py_4P·Zn_4-c-Tet1b** (38 mg, 85%) (Found: C, 68.75; H, 4.9; N, 7.1. $C_{264}H_{224}N_{24}O_{32}Zn_5$ requires C, 69.4; H. 4.9; N, 7.35%); δ_H(400 MHz; $CDCl_3$) 2.13 (8 H, d), 2.47 (24 H, s), 2.52 (24 H, s), 3.07–3.20 (32 H, m), 3.47 (24 H, s), 3.77 (24 H, s), 4.77 (32 H, br m), 5.85 (8 H, d), 7.04 (8 H, s), 7.77 (8 H, t), 7.99 (8 H, d), 8.14 (8 H, d), 8.50 (8 H, s), 10.13 (8 H, s); δ_C(100 MHz; $CDCl_3$) 15.2, 16.0, 22.0, 37.1, 51.5, 51.7, 74.8, 83.3, 97.1, 116.2, 117.8, 121.1, 127.5, 127.9, 130.7, 131.0, 134.8, 137.7, 138.3, 140.9, 141.1, 144.0, 146.0, 146.0, 146.3, 147.3, 147.4, 148.1, 149.4, 173.4 and 173.7.

H_2-Py_4P·Zn_4-c-Tet1b. Zn_4-c-Tet1b (38 mg, 10 μmol) and **H_2-Py_4P** (10 mg, 16 μmol) were dissolved in $CHCl_3$ (75 cm^3) and the procedure as outlined for **Zn-Py_4P·Zn_4-c-Tet1b** was followed to give **H_2-Py_4P·Zn_4-c-Tet1b** after recrystallisation from $CHCl_3$–MeOH (35 mg, 76%); δ_H(250 MHz; $CDCl_3$) −4.86 (2 H, s), 2.26 (8 H, d), 2.40 (24 H, s), 2.44 (24 H, s), 3.06 (32 H, m), 3.42 (24 H, s), 3.70 (24 H, s), 4.25 (32 H, br m), 5.77 (8 H, d), 6.88 (8 H, s), 7.72 (8 H, t), 7.93 (8 H, d), 8.07 (8 H, d), 8.43 (8 H, d) and 10.05 (8 H, s); δ_C(100 MHz; $CDCl_3$) 15.2, 16.0, 22.1, 29.7, 30.1, 37.1, 51.5, 51.7, 74.9, 83.3, 97.1, 115.5, 117.6, 121.1, 127.5, 127.9, 131.0, 134.8, 137.8, 138.3, 140.9, 141.2, 141.4, 144.0, 146.0, 146.4, 147.3, 147.4, 148.1, 148.3, 148.6, 173.3 and 173.7.

Acknowledgements

We thank the SERC, Magdalene and Trinity Colleges, Cambridge and Rhône-Poulenc-Rorer for financial support, and Kratos for MALDITOF spectra.

‡‡ $ZnPy_4P$ is much more soluble in MeOH than the cyclic tetramer complex, so a slight excess of ligand was used during recrystallisation to ensure complete complexation.

References

1 H. L. Anderson and J. K. M. Sanders, *J. Chem. Soc., Perkin Trans. 1*, 1995, preceding paper.
2 S. Anderson, H. L. Anderson and J. K. M. Sanders, *J. Chem. Soc., Perkin Trans. 1*, 1995, following paper.
3 S. Anderson, H. L. Anderson and J. K. M. Sanders, *Acc. Chem. Res.*, 1993, **26**, 469.
4 C. J. Walter, H. L. Anderson and J. K. M. Sanders, *J. Chem. Soc., Chem. Commun.*, 1993, 458; C. J. Walter and J. K. M. Sanders, *Angew. Chem., Int. Ed. Engl.*, 1995, **34**, 217.
5 L. G. Mackay, R. S. Wylie and J. K. M. Sanders, *J. Am. Chem. Soc.*, 1994, **116**, 3141.
6 H. L. Anderson and J. K. M. Sanders, *J. Chem. Soc., Chem. Commun.*, 1989, 1714.
7 H. L. Anderson and J. K. M. Sanders, *Angew. Chem., Int. Ed. Engl.*, 1990, **29**, 1400.
8 H. L. Anderson, R. P. Bonar-Law, L. G. Mackay, S. Nicholson and

J. K. M. Sanders *Supramolecular Chemistry*, ed V. Balzani and L. de Cola, Kluwer 1992, 359.
9 H. L. Anderson, C. A. Hunter, M. N. Meah and J. K. M. Sanders, *J. Am. Chem. Soc.*, 1990, **112**, 5780.
10 H. L. Anderson, *Inorg. Chem.*, 1994, **33**, 972.
11 A. J. Kirby, *Adv. Phys. Org. Chem.*, 1980, **17**, 183; L. Mandolini, *Adv. Phys. Org. Chem.*, 1986, **22**, 1.
12 C. B. Storm, A. H. Turner and M. B. Swann, *Inorg. Chem.*, 1984, **23**, 2743.
13 F. A. Walker and M. Benson, *J. Am. Chem. Soc.*, 1980, **102**, 5530.
14 J. K. M. Sanders and B. K. Hunter, *Modern NMR spectroscopy: a guide for chemists*, Oxford University Press, Oxford, 1993, 2nd edn.
15 H. Biedermann and K. Wichmann, *Z. Naturforsch, Teil B*, 1974, **29**, 360.
16 F. Kröhnke, *Synthesis*, 1976, 1.
17 R. Awartani, K. Sakizadeh and B. Gabrielsen, *J. Chem. Ed.*, 1986, **63**, 172.
18 W. H. Press, B. P. Flannery, S. A. Tenkolsky and W. T. Vetterling, *Numerical Recipes in Pascal*, Cambridge University, Press, 1989.
19 K. A. Connors, *Binding Constants*, Wiley, Chichester, 1987, p. 51.
20 B. D. Berezin, *Coordination Compounds of Porphyrins and Phthalocyanines*, Wiley, Chichester, 1981, p. 62; P. Hambright, *J. Chem. Soc., Chem. Commun.*, 1967, 470.
21 D. W. J. McCallien and J. K. M. Sanders, *J. Am. Chem. Soc.*, 1995, **117**, 6611.
22 I. P. Danks, I. O. Sutherland and C. H. Yap, *J. Chem. Soc., Perkin Trans 1*, 1990, 421.
23 C. A. Hunter, M. N. Meah and J. K. M. Sanders, *J. Am. Chem. Soc.*, 1990, **112**, 5773.
24 A. V. Hill, *J. Physiol. London*, 1910, **40**, IV-VII.
25 D. Seebach, E. Hungerbüler, R. Naef, P. Schnurrenberger, B. Weidmann and M. Züger, *Synthesis*, 1982, 138.
26 S. Anderson, H. L. Anderson, A. Bashall, M. McPartlin and J. K. M. Sanders, *Angew. Chem., Int. Ed. Engl.*, 1995, **34**, 1096.
27 H. L. Anderson, A. Bashall, K. Henrick, M. McPartlin and J. K. M. Sanders, *Angew. Chem., Int. Ed. Engl.*, 1994, **33**, 429.
28 M. I. Page and W. P. Jencks, *Proc. Nat. Acad. Sci. USA*, 1971, **68**, 1678; W. P. Jencks, *Proc. Nat. Acad. Sci. USA*, 1981, **78**, 4046.

Paper 5/01072A
Received 22*nd February* 1995
Accepted 1*st June* 1995